Available online at www.sciencedirect.com
ScienceDirect
Thin Solid Films 515 (2006) 1166–1170
www.elsevier.com/locate/tsf

Growth of epitaxial Cu on MgO(001) by magnetron sputter deposition

J.M. Purswani [a], T. Spila [b], D. Gall [a,*]

[a] Department of Materials Science and Engineering, Rensselaer Polytechnic Institute, Troy, NY 12180, USA
[b] Center for Microanalysis of Materials, University of Illinois, Urbana, IL 61801, USA

Available online 11 September 2006

Abstract

100-nm-thick Cu layers were grown on MgO(001) substrates by ultra-high vacuum magnetron sputter deposition at substrate temperatures T_s ranging from 40 to 300 °C. X-ray diffraction ω–2θ scans, ω-rocking curves, and pole figures show that layers grown at T_s=40 and 100 °C are complete single crystals with a cube-on-cube epitaxial relationship with the substrate: $(001)_{Cu}||(001)_{MgO}$ with $[100]_{Cu}||[100]_{MgO}$. In contrast, $T_s \geq 200$ °C leads to polycrystalline Cu layers with 001, 203, and $\bar{1}75$-oriented grains. The transition from a single- to a polycrystalline microstructure with increasing T_s is attributed to temperature-induced mass transport that allows Cu nuclei to sample a larger orientational space and find lower energy (and/or lower lattice mismatch) configurations. The large Cu- to-MgO lattice mismatch of 14% is relieved by 7×7 Cu unit cells occupying 6×6 MgO cells. In addition, for $T_s \geq 200$ °C, the 001-oriented grains relax by tilting by 4° or 15° about ⟨110⟩ or ⟨100⟩ axes, respectively, while the 203 and $\bar{1}75$-oriented grains exhibit complex epitaxial relationships with the substrate: $(203)_{Cu}||(001)_{MgO}$ with $[010]_{Cu}||[110]_{MgO}$ and $[30\bar{2}]_{Cu}||[1\bar{1}0]_{MgO}$; and $(\bar{1}75)_{Cu}||(001)_{MgO}$ with $[21\bar{1}]_{Cu}||[100]_{MgO}$ and $[4\bar{3}5]_{Cu}||[010]_{MgO}$. The surface roughness, as determined by X-ray reflectivity, increases with growth temperature. The smoothest layers are grown at 40 °C and exhibit an rms surface and buried interface roughness of 0.7 and 1.4 nm, respectively.

Keywords: Copper; Epitaxy; Sputter deposition

1. Introduction

The growth of epitaxial copper thin films with thicknesses $t \leq 100$ nm is required to study the electron transport in Cu at reduced length scales and in the absence of grain-boundaries. Of particular interest is the electron-scattering at the surface, which contributes to the so called "size effect" [1]. The size-effect refers to a resistivity increase which becomes important when the conductor line width reaches length scales comparable to the room-temperature electron mean free path, determined by electron-phonon scattering, of 39 nm [2]. The resistivity increase represents a major challenge for the continuous device scaling in integrated circuits as specified in the International Technology Roadmap for Semiconductors [3]. Studies on single crystal Cu layers are needed to determine the surface and barrier-layer requirements that lead to specular electron scattering, that is, will suppress the size effect.

Most work on the epitaxial growth of Cu has been done on H-terminated Si(001) and Si(111) surfaces [4–10], where the Cu layer grows with $(001)_{Cu}||(001)_{Si}$ and $[100]_{Cu}||[110]_{Si}$ on the Si(001) surface and with $(111)_{Cu}||(111)_{Si}$ on Si(111). However, for both systems, there are two possible orientations for the Cu nucleation, so that the resulting layer is highly twinned. Similarly, epitaxial growth of Cu(111) on the basal plane of sapphire leads to a twinned structure which is not a "true" single crystal [11–13]. In contrast, Cu growth on MgO(001) exhibits a cube-on-cube epitaxial relationship, $(001)_{Cu}||(001)_{MgO}$ with $[100]_{Cu}||[100]_{MgO}$, with only one possible crystalline orientation, yielding a Cu single crystal layer without twin boundaries [10,13–18]. Such a layer is clearly preferred for electron-transport studies, since twin boundary electron scattering is absent. Reported epitaxial Cu/MgO(001) growth temperatures T_s range from room temperature [10,14] to 185 °C [15], 50–300 °C [16], 300–350 °C [17], 370 °C [18], and 580 °C [13]. However, it is unclear what temperature yields the highest quality Cu layer since most studies determine the crystalline structure only by XRD ω–2θ scans and reflection high energy electron diffraction—techniques which are relatively insensitive to

* Corresponding author. Tel.: +1 518 276 8471.
E-mail address: galld@rpi.edu (D. Gall).

0040-6090/$ - see front matter © 2006 Elsevier B.V. All rights reserved.
doi:10.1016/j.tsf.2006.07.142

small but important concentrations of misoriented grains. In addition, it is still unclear how the large (14%) lattice mismatch between Cu and MgO affects epitaxial growth, including the reported temperature dependent surface morphology which indicates a 3D Stranski–Krastanov growth mode [6,10,13,16].

Here we report on the growth of epitaxial Cu layers, deposited directly on MgO(001) substrates by ultra-high vacuum magnetron sputtering. X-ray diffraction (XRD) ω−2θ, ω-rocking curves, and pole figures show that layers grown at temperatures $T_s \leq 100$ °C are complete single crystals while $T_s \geq 200$ °C leads to polycrystalline films. The latter consist of grains with various crystalline orientations that exhibit well defined (epitaxial) orientation relationships with the substrate. The transition from a single- to a polycrystalline microstructure with increasing T_s is attributed to temperature-induced mass transport that allows Cu nuclei to sample a larger orientational space and find lower energy (lower lattice mismatch) configurations. An observed grain tilt indicates that cube-on-cube epitaxy of Cu on MgO(001) is possible because the large lattice mismatch is compensated by a growth where 7 Cu-unit cells nucleate of 6 MgO cells. X-ray reflectivity shows that the surface and interface roughness increases with increasing growth temperature.

2. Experimental procedure

All Cu layers were grown in a load-locked multi-chamber UHV stainless-steel dc magnetron sputter deposition system with a base pressure of 1.3×10^{-7} Pa (1×10^{-9} Torr), achieved using a 520 l-s^{-1} turbomolecular pump. The substrates were polished $10\times10\times0.5$ mm^3 MgO(001) wafers (99.99%) cleaned with successive rinses in ultrasonic baths of trichloroethylene, acetone, isopropanol, and deionized water and blown dry with dry N_2 [19]. The wafers were then mounted on a molybdenum holder and inserted into the sample introduction chamber for transport to the growth chamber where they were thermally degassed at 800 °C for 1 h. 99.999% pure Ar was further purified using a Micro Torr purifier and introduced through metering valves to reach a constant chamber pressure of 0.33 Pa (2.5 mTorr), which was measured using a capacitance manometer. A water-cooled 7.5-cm-diameter Cu target with a purity of 99.999% was facing the substrate with a source-substrate-distance of 25 cm. Just prior to initiating deposition, the target was sputter cleaned for 5 min while the substrate was covered with a protective disc. Sputtering was carried out at a constant power of 150 W, yielding a deposition rate of 10 nm/min. The film growth temperature T_s=40, 100, 200, 300 °C, including the contribution due to plasma heating, was measured by a thermocouple within the sample stage that was cross-calibrated with a pyrometer at higher temperatures. Following deposition, the samples were allowed to cool to <50 °C before being transferred to the load lock chamber which was then vented with dry N_2.

The crystalline structure and quality of the Cu layers were analyzed by X-ray diffraction (XRD) techniques. Both ω–2θ scans and ω-rocking curves were collected using a Rigaku D-MAX powder diffractometer system with a CuK$_\alpha$ source and slit divergences of 1° for ω–2θ scans and ω-rocking curves, respectively, giving rise to resolutions of 0.01 °2θ. The complete crystalline orientation information was obtained by 002, 111, and 311 pole figure measurements using a four-circle Philips X-pert MRD diffractometer operated at 45 kV and 40 mA with a 1×1 mm^2 point-focus Cu X-ray source and secondary optics equipped with a parallel plate collimator, a flat graphite crystal monochromator, and a proportional detector. X-ray reflectivity (XRR) measurements were performed using a high-resolution Philips X-pert MRD diffractometer with a Cu K$_{\alpha_1}$ source (λ=0.1540597 nm) and a four-crystal Ge(220) monochromator which provides an angular beam divergence of <12 arc sec with a wavelength spread $\Delta\lambda/\lambda=7\times10^{-5}$.

3. Results

Fig. 1(a) shows a portion of X-ray diffraction ω–2θ scans from Cu layers grown on MgO(001) at T_s=40, 100, 200, and 300 °C. For all layers in this study, the only observable peaks in the measured scan range from 44–130 °2θ are the Cu 002 and Cu 004 reflections, as well as the MgO 002 and 004 substrate peaks. The Cu 002 reflection at 50.62° is above the expected value of 50.45°, indicating a slight tensile stress causing a in-plane strain, determined using a Poisson ratio ν_{Cu}=0.33, of ε_2=0.3% which is attributed to the lattice misfit between layer and substrate. The full width at half maximum (FWHM) of the Cu 002 peak, $\Gamma_{2\theta}$=0.45°, is nearly independent of T_s and is attributed to a combination of broadening due to the limited

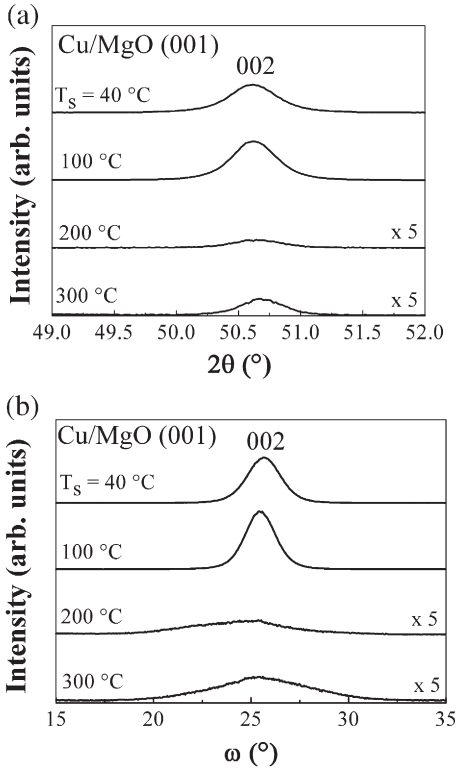

Fig. 1. (a) X-ray diffraction ω–2θ scans from 100-nm-thick Cu/MgO(001) layers grown at 40, 100, 200, and 300 °C with (b) ω-rocking curves from the Cu 002 reflection at 50.62°.

layer thickness (contributing a broadening of 0.13°) and lateral variations in the strain-state. The peak intensity strongly depends on the growth temperature, and drops by more than an order of magnitude from 14,500 and 20,000 counts per second (cps) for 40 and 100 °C, respectively, to 450 and 900 cps for 200 and 300 °C, respectively. This indicates a higher crystalline quality and/or orientation alignment for the Cu layers grown at lower temperatures, with the highest layer quality for $T_s = 100$ °C. This conclusion is supported by the ω-rocking curves of the Cu 002 peaks, shown in Fig. 1(b). The FWHM values are 2.0 and 1.8° for 40 and 100 °C, but increased to 5.5° for both 200 and 300 °C. That is, all layers exhibit a preferred orientation (in contrast to a random grain orientation) with $(001)_{Cu}\|(001)_{MgO}$. However, the layers grown at $T_s \leq 100$ °C show a much stronger crystalline alignment with the substrate, as compared to layers grown at $T_s \geq 200$ °C. The wide rocking curves for $T_s \geq 200$ °C are associated with a tilt of the Cu grains to relieve misfit strain, as discussed below.

Fig. 2 shows XRD pole figure maps from 100-nm-thick Cu layers grown at 100 and 200 °C, obtained with constant 2θ values corresponding to the Cu 002 and Cu 111 reflections at $2\theta = 50.42°$ and 43.32°, respectively. All measured pole figures, including the 002, 111, and 311, from Cu layers grown at $T_s = 40$ °C are identical to those for $T_s = 100$ °C shown in Fig. 2. Similarly, $T_s = 200$ and 300 °C yield similar pole figures. That is, the data shown in Fig. 2 is representative for $T_s \leq 100$ °C (a, b) and $T_s \geq 200$ °C (c, d).

The 002-pole figure in Fig. 2(a) from a Cu layer grown at $T_s = 100$ °C exhibits a single peak at the origin. The absence of any other peaks indicates that all grains in the Cu layer have their (001)-plane parallel to the substrate surface, that is, parallel to the MgO(001). The 111-pole figure in Fig. 2(b) from the same Cu layer has four symmetric peaks at a tilt-angle $\psi = 54.7°$ and at polar angles $\phi = 45°$, 135°, 225°, and 315°. The angle between [111] and [001] in cubic materials is 54.7°, that is, these four peaks emanate from Cu with $(001)_{Cu}\|(001)_{MgO}$. In addition, the polar angles indicate that $[001]_{Cu}\|[001]_{MgO}$. Thus, the Cu grows with a cube-on-cube epitaxial relationship with the substrate for layers with $T_s \leq 100$ °C.

Fig. 2(c) is the 002-pole figure from a Cu layer with $T_s = 200$ °C. It exhibits, in addition to the peak at the origin, three strong sets of peaks at $\psi = 15°$, 35°, and 55°. The peak at the origin, in contrast to that shown in Fig. 2(a), is non-circular with elongations to $\psi \approx 4°$ along 4-fold symmetric directions with $\phi = 45°$, 135°, 225°, and 315°. These elongations are attributed to a tilt of the Cu grains to relieve misfit strain. The misfit of Cu ($a = 0.3615$ nm) on MgO ($a = 0.4213$ nm) is $(a_{MgO} - a_{Cu})/a_{MgO} = 14.19\%$, which is very close to $1/7 = 14.29\%$. That is, epitaxy is achieved by 7 Cu unit cells fitting onto 6 MgO cells. However, the fit can be improved by a slight tilt of the Cu(001) plane with respect to the MgO(001). We calculate an optimal tilt angle about a ⟨100⟩ axis of $\gamma = \cos^{-1}(6 \cdot a_{MgO}/7 \cdot a_{Cu}) = 2.6°$, which leads, if tilt occurs on both orthogonal [100] and [010] axes, to a total tilt of 3.7° about the ⟨110⟩ axis, in perfect agreement with the observed 4° tilt at $\phi = 45°$, 135°, 225°, and 315°.

The set of peaks observed at $\psi = 15°$ are also associated with tilted 001-oriented Cu grains, however, in this case 5 Cu unit cells fit on 6 MgO cells. Using the above lattice constants for Cu and MgO and $\cos\gamma = 5 \cdot a_{MgO}/6 \cdot a_{Cu}$, we calculate a tilt-angle corresponding to a rotation about ⟨100⟩ axes of 13.8°, in good

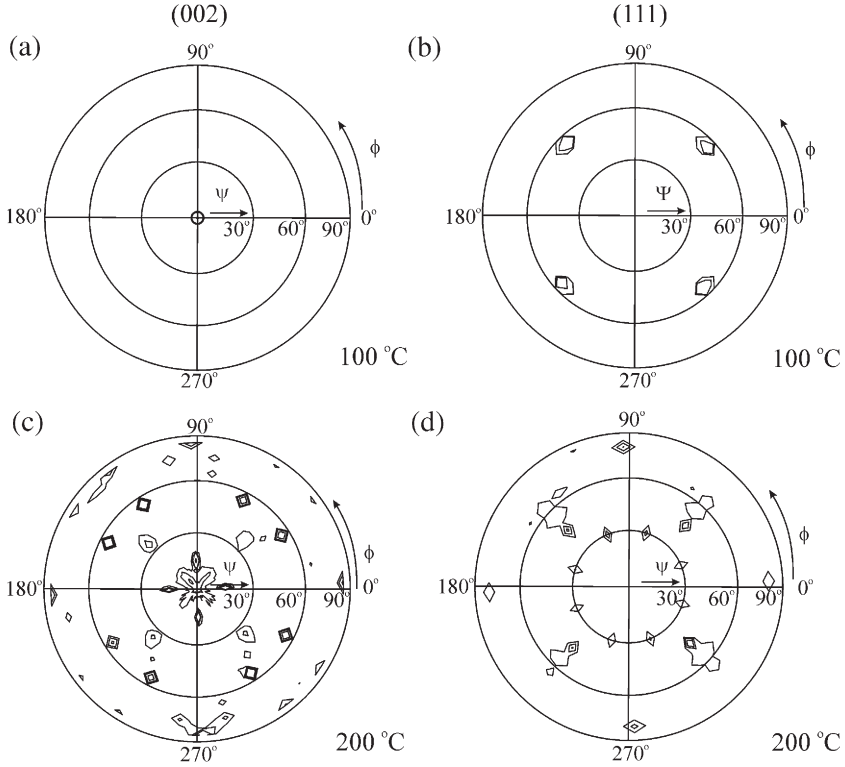

Fig. 2. XRD pole figures from Cu/MgO(001) layers grown at (a,b) 100 and (c,d) 200 °C, using (a,c) Cu 002 and (b,d) Cu 111 reflections.

agreement with the observed $\psi = 15°$ and $\phi = 0°$, 90°, 180°, and 270°. In addition, these grains are expected to give rise to peaks at $\psi = 90° - 15° = 75°$. They are observed at a slightly higher angle $\psi \approx 80°$ with $\phi = 0°$, 90°, 180°, and 270°. The discrepancy in ψ is attributed to the large uncertainty during pole figure measurements at high tilt-angles. Also, these tilted grains are observed in the 111 pole figure, showing a strong elongation (by $\approx \pm 15°$) along ψ for the peaks at $\psi_{111} = 54.7°$ and $\phi = 45°$, 135°, 225°, and 315°.

The four peaks at a tilt angle of $\psi_{002} = 35°$ in Fig. 2(c) are attributed to grains with a 203-orientation, which give also rise to peaks at $\psi_{111} = 81°$ in the 111 pole figure in Fig. 2(d). An alternative assignment using 112-oriented grains could explain the ψ_{002} and ϕ_{002} values but not the ψ_{111}. The 203-oriented grains exhibit a 45° rotated epitaxial relationship with the substrate, that is, $(203)_{Cu}||(001)_{MgO}$ with $[010]_{Cu}||[110]_{MgO}$ and $[30\bar{2}]_{Cu}||[1\bar{1}0]_{MgO}$. This arrangement leads a 1.1% lattice mismatch along $[110]_{MgO}$ and a 0.5% mismatch along $[1\bar{1}0]_{MgO}$, using ratios of Cu unit cells versus diagonal MgO unit cells of 3/5 and 4/9, respectively.

The eight peaks at $\psi_{002} = 55°$ with $\phi_{002} = 30°$, 60°, 120°, 150°, 210°, 240°, 300°, and 330° are attributed to $\bar{1}75$-oriented Cu grains which also result in eight peaks in the 111 pole figure at $\psi_{111} = 30°$. Their epitaxial relationship with the substrate is as follows: $(\bar{1}75)_{Cu}||(001)_{MgO}$ with $[21\bar{1}]_{Cu}||[100]_{MgO}$ and $[4\bar{3}5]_{Cu}||[010]_{MgO}$. The same crystalline relationship has previously been reported for the growth of Ni on MgO(001), which leads to a c(3 × 1) surface lattice [19]. In the present case, the $\bar{1}75$-oriented Cu grains have a lattice mismatch with the substrate of 4.8% in the $[21\bar{1}]_{Cu}$ and a 1.1% mismatch along $[4\bar{3}5]_{Cu}$.

Fig. 3 shows X-ray reflectivity results from Cu/MgO(001) layers grown at 40 and 100 °C, that is, from layers that have been determined by XRD pole figure measurements to be single crystals. The plot from the sample with $T_s = 40$ °C (offset by 1.5 decades for clarity) shows strong interference fringes between 0.5 and 1.2 °2θ from the reflection at the air/Cu and Cu/MgO interfaces. The fringes are less pronounced for $T_s = 100$ °C, but still observable between 0.6 and 0.8 °2θ. The decreased fringe intensity is attributed to an increase in surface and/or interface roughness with increasing T_s, in agreement with scanning tunneling microscopy studies which indicate an increasing surface roughness with increasing T_s [16]. The inset in Fig. 3 shows a portion of the plot for $T_s = 40$ °C, including a fit to the data obtained using the full 0.25–3.0 °2θ range. The fringe spacing provides an accurate measurement of the Cu layer thickness $t = 99 \pm 2$ nm, which is in excellent agreement with the nominal thickness of 100 nm, obtained from cross-sectional scanning electron microscopy growth rate calibrations. The fit also provides values, based on the intensity decay and fringe amplitude, for the root mean square surface and buried Cu/MgO interface roughness of 0.7 and 1.4 nm, respectively.

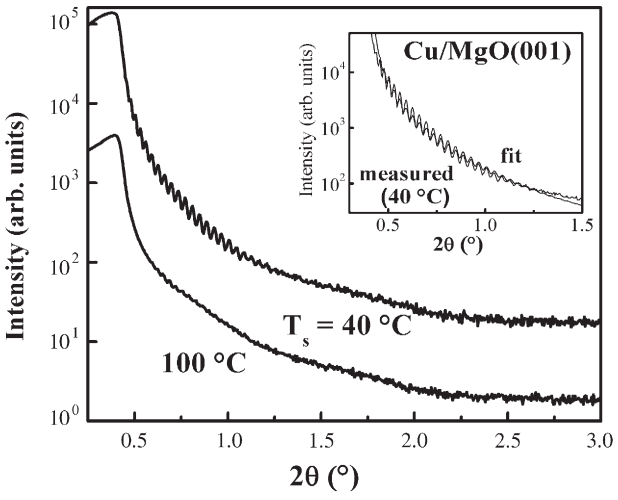

Fig. 3. Plot of X-ray reflectivity intensity (offset for clarity) for Cu/MgO(001) layers grown at 40 and 100 °C. The inset shows a portion of the $T_s = 40$ °C scan, including a fit to the data.

4. Discussion

X-ray diffraction analyses indicate a clear transition in the epitaxial growth mode of Cu on MgO(001) as a function of growth temperature T_s. In particular, when comparing layers with $T_s \leq 100$ °C to layers with $T_s \geq 200$ °C, the low-temperature layers exhibit (a) an approximately 20× higher intensity of the Cu(002) peak in ω–2θ scans, (b) a 3× narrower ω-rocking curve, and (c) a single set of peaks in the 002 and 111 pole figures. The combination of these results shows that layers with $T_s \leq 100$ °C are single crystals with a cube on cube epitaxial relationship with the substrate $(001)_{Cu}||(001)_{MgO}$ with $[100]_{Cu}||[100]_{MgO}$. They exhibit full widths at half maximum of the ω-rocking curves of 2.0 and 1.8° for $T_s = 40$ and 100 °C, respectively. These values are in good agreement with a previously reported rocking curve width of 1.8°, obtained from a 100-nm-thick Cu/MgO(001) layer grown at 142 °C [10]. The slight decrease in mosaicity with increasing T_s, indicating an increasing crystalline quality, is attributed to a temperature induced enhancement of the adatom mobilities which reduces the number of point defects and increases the lateral length scale for mound nucleation. However, a further increase in T_s to 200 and 300 °C does not lead to narrower ω-rocking curves but a dramatic broadening, with a FWHM of 5.5°. The broadening is attributed to a tilting of 001-oriented Cu to relieve misfit strain, as determined from pole figure analyses, similar to a reported tilt of Cu grains on Ge(001) [6]. Cu has a 14.19% smaller lattice constant than MgO. This large lattice mismatch is nearly completely compensated when 7 × 7 Cu unit cells occupy 6 × 6 MgO cells, yielding a remaining mismatch of 0.1% which, in turn, is relieved by tilting the Cu grain by 4° about a ⟨110⟩ axis. An alternative relaxation is achieved when 6 × 7 Cu unit cells occupy 5 × 6 MgO cells. In that case, the 5/6 ratio yields a remaining mismatch of 3.0%, which is compensated by tilting Cu grains by 15° about a ⟨100⟩ axis. These two modes for tilt-relaxation are only observed for layers grown at $T_s \geq 200$ °C. This is an indication that considerable (temperature activated) atomic mass transport is required to cause tilts, which likely occur on relatively large (10–1000 nm) length scales. The detection of tilted grains at $T_s \geq 200$ °C provides insight into the epitaxial growth of Cu/MgO(001), independent of T_s. In

particular, it shows that the 14% lattice mismatch is compensated by the mapping of 7×7 Cu unit cells onto 6×6 MgO cells. We expect this to be also the case for $T_s \leq 100$ °C, yielding nearly no misfit stress in the Cu layer, in agreement with the measured in-plane tensile strain ε_2 of only 0.3%.

The Cu layers with $T_s \geq 200$ °C exhibit, in addition to the tilted 001-grains, also 203 and $\bar{1}75$-oriented Cu grains. Both grain orientations exhibit an epitaxial relationship with the substrate, as determined by combining 002 and 111 pole figure data: $(203)_{Cu}||(001)_{MgO}$ with $[010]_{Cu}||[110]_{MgO}$ and $[30\bar{2}]_{Cu}||[1\bar{1}0]_{MgO}$ yielding a misfit along perpendicular $\langle 110\rangle_{MgO}$ directions of 0.5 and 1.1%; and $(\bar{1}75)_{Cu}||(001)_{MgO}$ with $[21\bar{1}]_{Cu}||[100]_{MgO}$ and $[4\bar{3}5]_{Cu}||[010]_{MgO}$ with a calculated misfit of 4.8% and 1.1% in perpendicular directions. The calculated misfit alone does not explain the presence of these orientations, since the cube-on-cube epitaxial Cu layer with a 7/6 unit cell ratio with the MgO substrate has even a lower misfit. However, the latter has a relatively large 2D interface unit cell of 6×6 $(a_{MgO})^2 = 640$ Å^2, which results in a reduced likelihood for epitaxy.

5. Conclusions

In summary, we explain the transition in the epitaxial growth mode as a function of T_s as follows: at low temperatures, Cu atoms on a MgO(001) surface have limited mobility and tend to occupy low energy sites above O-atoms [14], which leads to the formation of Cu(001) islands with a cube-on-cube epitaxy. As islands grow, the increasing strain leads to the formation of misfit dislocations which ultimately results in an epitaxial system where 7×7 Cu cells occupy 6×6 MgO cells, leading to a nearly strain-free single crystal layer. However, at $T_s \geq 200$ °C, the larger atomic mobility allows strained cube-on-cube islands to sample tilted structures as well as completely different crystalline orientations, some of which are energetically favorable over the strained 001-island. Consequently, a polycrystalline layer nucleates where all grains exhibit a well defined epitaxial relationship with the substrate.

Acknowledgements

This research was funded by the Semiconductor Research Corporation (SRC) and New York State through the Center for Advanced Interconnect Systems Technologies (CAIST) under contract number 1292.004. X-ray diffraction and reflectivity techniques were carried out in the Center for Microanalysis of Materials, University of Illinois, which is partially supported by the U.S. Department of Energy under grant DEFG02-91-ER45439.

References

[1] S.M. Rossnagel, T.S. Kuan, J. Vac. Sci. Technol. B 22 (2004) 240.
[2] T.S. Kuan, C.K. Inoki, G.S. Oehrlein, K. Rose, Y.-P. Zhao, G.-C. Wang, S.M. Rossnagel, C. Cabral, Mater. Res. Soc. Symp. Proc. 612 (2000) D7.1.1.
[3] http://public.itrs.net/.
[4] E.T. Krastev, L.D. Voice, R.G. Tobin, J. Appl. Phys. 79 (9) (1996) 6865.
[5] I. Hashim, B. Park, H.A. Atwater, Appl. Phys. Lett. 63 (20) (1993) 2833.
[6] B. Karr, Y.W. Kim, I. Petrov, D.B. Bergstrom, D.G. Cahill, J.E. Greene, L.D. Madsen, J.-E. Sundgren, J. Appl. Phys. 80 (12) (1996) 6699.
[7] H. Jiang, T.J. Klemmer, J.A. Barnard, E.A. Payzant, J. Vac. Sci. Technol., A 16 (6) (1998) 3376.
[8] T.I.M. Bootsma, T. Hibma, Surf. Sci. 331–333 (1995) 636.
[9] I. Hashim, B. Park, H.A. Atwater, Mater. Res. Soc. Symp. Proc. 280 (1993) 327.
[10] T. Mewes, M. Rickhart, A. Mougin, S.O. Demokritov, J. Fassbender, B. Hillebrands, M. Scheib, Surf. Sci. 481 (2001) 87.
[11] G. Dehm, M. Rühle, G. Ding, R. Raj, Philos. Mag., B 71 (6) (1995) 1111.
[12] G. Katz, Appl. Phys. Lett. 12 (5) (1968) 161.
[13] H. Bialas, K. Heneka, Vacuum 45 (1) (1994) 79.
[14] J.-W. He, P.J. Møller, Surf. Sci. 178 (1986) 934.
[15] H. Qiu, Y. Tian, M. Hashimoto, J. Univ. Sci. Technol. Beijing 8 (3) (2001) 207.
[16] G. Eilers, K. Mukasa, Jpn. J. Appl. Phys. 39 (2000) 3780.
[17] M.P. Delplancke, P. Delcambe, L. Binst, M. Jardinier-Offergeld, F. Bouillon, Thin Solid Films 143 (1986) 43.
[18] F. Reniers, M.P. Delplancke, A. Asskali, V. Rooryck, O. Van Sinay, Appl. Surf. Sci. 92 (1996) 35.
[19] E.B. Svedberg, P. Sandström, J.-E. Sundgren, J.E. Greene, L.D. Madsen, Surf. Sci. 429 (1999) 206.